*Perspective*

# Redox Activity as a Powerful Strategy to Tune Magnetic and/or Conducting Properties in Benzoquinone-Based Metal-Organic Frameworks

**Noemi Monni** [1,2,*], **Mariangela Oggianu** [1,2], **Suchithra Ashoka Sahadevan** [3] **and Maria Laura Mercuri** [1,2,*]

1   Department of Chemical and Geological Sciences, University of Cagliari, Highway 554, Crossroads for Sestu, I09042 Monserrato (CA), Italy; mari.oggianu@gmail.com
2   National Interuniversity Consortium of Materials Science and Technology, INSTM, Street Giuseppe Giusti, 9, I50121 Florence, Italy
3   Applied Physical Chemistry, Centre of Molecular Devices, Department of Chemistry, KTH Royal Institute of Technology, SE-10044 Stockholm, Sweden; suchithraiiserk@gmail.com
*   Correspondence: noemi.monni@unica.it (N.M.); mercuri@unica.it (M.L.M.)

**Abstract:** Multifunctional molecular materials have attracted material scientists for several years as they are promising materials for the future generation of electronic devices. Careful selection of their molecular building blocks allows for the combination and/or even interplay of different physical properties in the same crystal lattice. Incorporation of redox activity in these networks is one of the most appealing and recent synthetic strategies used to enhance magnetic and/or conducting and/or optical properties. Quinone derivatives are excellent redox-active linkers, widely used for various applications such as electrode materials, flow batteries, pseudo-capacitors, etc. Quinones undergo a reversible two-electron redox reaction to form hydroquinone dianions via intermediate semiquinone radical formation. Moreover, the possibility to functionalize the six-membered ring of the quinone by various substituents/functional groups make them excellent molecular building blocks for the construction of multifunctional tunable metal-organic frameworks (MOFs). An overview of the recent advances on benzoquinone-based MOFs, with a particular focus on key examples where magnetic and/or conducting properties are tuned/switched, even simultaneously, by playing with redox activity, is herein envisioned.

**Keywords:** metal-organic frameworks; redox; magnetism; conductivity; benzoquinones; semiquinones

## 1. Introduction

Over several decades, metal-organic frameworks (MOFs) have been extensively studied [1] due to their unique supramolecular architectures, which lead to high porosity and interesting properties in magnetism [2], conductivity [3], photochromism [4,5], luminescence [6–9], etc. MOFs are coordination compounds formed by metal ions linked to organic ligands, forming an infinite array in one, two, or three dimensions (1D, 2D, and 3D) and offering a plethora of applications in different fields including gas storage, separation, catalysis, energy storage, sensing, biomedical applications, etc. [10–14]. Depending on a careful choice of metal ions/linkers [15], MOFs can also show a combination and/or even interplay of physical properties. A relatively new strategy [10,16,17] to enhance their physical properties, in particular, magnetism and conductivity, is the incorporation of redox activity. Redox activity can be promoted via various methods such as (*i*) a rational design of redox-active metals centers or linkers [18], (*ii*) post-synthetic modifications of metal ions or through ligand exchange, and (*iii*) encapsulation of redox-active guest ions in the pores of MOFs [19], leading to the formation of radical species, affecting the electronic properties of the organic linkers and, therefore, the physical properties of the related networks [20,21]. Among the redox-active linkers, derivatives of pyrazine [22], dithiolenes [23], triphenylamine [24], N,N-Dipyridil Naphthalenediimide [20], hexaaminobenzene [25], por-

phyrin [26], bipyridine [27], etc., are most commonly used in MOFs, while multidentate redox- active linkers, providing different possibilities to tune redox activity, still represent a challenge up to now [20,21,28].

The benzoquinone/hydroquinone linkers represent a redox-active couple remarkably studied in technologically important materials such as electrodes [6,29], flow batteries [30], pseudo-capacitors [31], and materials used in artificial photosynthesis [32]. Benzoquinones are a class of naturally occurring organic compounds that possess two carbonyl groups C=O in the 1 and 4 position in an unsaturated six-membered ring [33]. Benzoquinones are usually electron deficient, and their benzoquinoid-like configuration undergoes a mono-electron reversible reduction to produce the para semiquinone radical species, which, in turn, could be further reduced to form the aromatic hydroquinone dianion (*vide infra*), as described in Scheme 1.
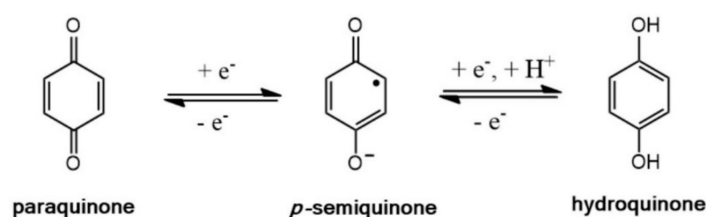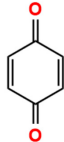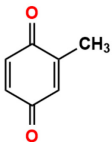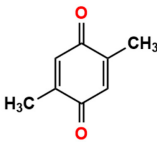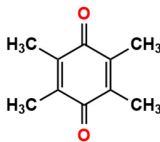


**Scheme 1.** Reversible redox reactions for *p*–quinone/hydroquinone couple.

The stability of the semiquinoid form could be influenced by different factors, such as the nature of the ring substituents, intra/intermolecular hydrogen bonding, solvent polarity, the presence of acidic or basic additives, and protonation [34–39]. Particularly, chemical tailoring of benzoquinone linkers, through the functionalization of the six-membered ring by various substituents (halo, nitro, amino, methoxy, etc.), can stabilize the radical anion [40], depending on the steric and electronic nature of the substituents, thus modulating the physical properties of the benzoquinone-based networks at a molecular level [41]. In fact, the presence of different substituents on the benzoquinoid ring can tune the one-electron reduction potential, as shown in Table 1. When the benzoquinones are functionalized with electron-donating substituents, i.e., methyl groups, the reduction potential is more negative depending on how many methyl groups are present, making these species more difficult to reduce. On the contrary, it is possible to observe an opposite trend when electron-withdrawing substituents, such as chlorine, are present. Therefore, benzoquinones co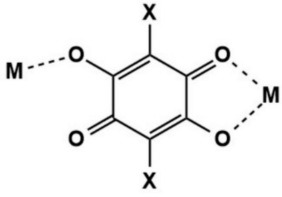ntaining chlorine substituents in the ring show more positive reduction potentials and consequently are easier to reduce [33].

Among the parabenzoquinones derivatives, 2,5-dihydroxy-1,4-benzoquinones (dhbq) have attracted ever-growing interest in material chemistry due to their versatile coordination modes (Scheme 2). Furthermore, when hydrogens at the 3 and 6 position are replaced with different substituents (halogen atoms or functional groups), they are better known in the literature as anilic acids, formulated as $H_2X_2C_6O_4$ ($H_2X_2An$), where X indicates the substituent and $C_6O_4$ indicates the anilate moiety (An) [2,42,43]. When the anilic acids are in their dianionic form, i.e., anilates, they act as valuable linkers for transition [44–51] and lanthanide metal nodes [52–58] to build materials showing a combination of fascinating physical properties and redox states (*vide infra*). All these features make them interesting molecular building blocks for constructing a large variety of novel supramolecular frameworks [49,59], as shown in Figure 1. Particularly, most of the reported structures based on parabenzoquinone derivatives are 2D, paving the way for a further exfoliation of bulk MOFs to fabricate metal-organic nanosheets (MON) that can show peculiar redox behavior [60].

**Table 1.** Theoretical one-electron reduction potentials of selected benzoquinone derivatives (mV vs. NHE in CH$_3$CN) [61] showing the influence of substituents.

| Benzoquinone Derivatives (E$_{NHE}$) |
| :---: |



1,4-benzoquinone (−255 mV)



| 2-methylbenzoquinone (−341 mV) | 2,5-dimethylbenzoquinone (−434 mV) | 2,3,5,6-tetramethylbenzoquinone (−646 mV) |
| :---: | :---: | :---: |



| 2-chlorobenzoquinone (−139 mV) | 2,5-dichlorobenzoquinone (33 mV) | 2,3,5,6-tetrachlorobenzoquinone (837 mV) |
| :---: | :---: | :---: |
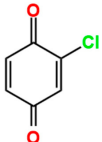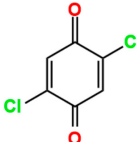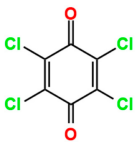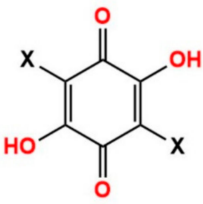


X = H, Cl, Br, I, CN, *etc.*

**3,6-disubstituted-2,5-dihydroxy-1,4-benzoquinone**
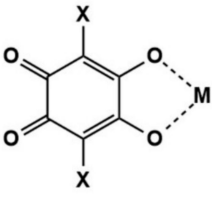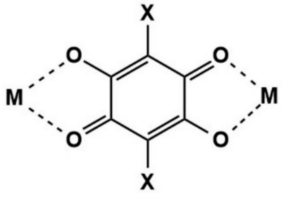


| 1,2-bidentate | bis-1,2-bidentate | 1,2-bidentate/monodentate |
| :---: | :---: | :---: |

**Scheme 2.** Chemical structure of anilates and the most common coordination modes.

On this basis, MOFs formed by metal nodes and benzoquinoid-based ligands, especially anilates, feature an ideal platform for the construction of porous redox materials with switchable conducting/magnetic properties [62], due to the changeover to the semiquinoid form.
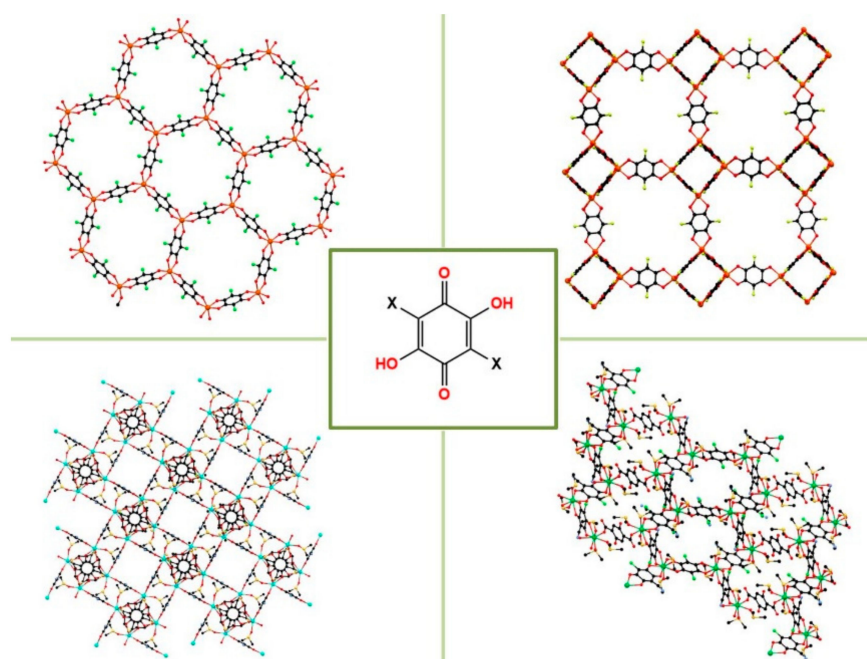
**Figure 1.** Extended networks based on anilates.

A pioneering study on a dhbq based-framework, reported by Abrahams et al. [63], revealed (*i*) the potential of benzoquinone to act as a suitable building block for constructing extended frameworks [64] and (*ii*) its capability to receive/lose electrons while keeping unchanged the supramolecular architecture. This study opened up unprecedented routes to tune the physical properties of extended frameworks through redox activity.

The present work focuses on key examples of the latest developments (from 2015 to date) on redox-active benzoquinone-based MOFs showing conducting and/or magnetic properties. The aim is to evidence the enhancement/switching of magnetism and/or conductivity due to a fine modulation of benzoquinone redox properties, highlighting the extreme versatility of this class of redox-active linkers in tailoring the physical properties of extended frameworks.

## 2. Semiquinone-Based MOFs

The incorporation of a semiquinone in a solid framework could be achieved through in situ or post-synthetic reduction of the benzoquinone derivatives. In 2016, Stock et al. [65] reported on the first example of permanently porous $Al^{III}$-MOFs, of the formulas $(CH_3)_2NH_2)_3$ $[Al_4(dhbq)_3(dhbq^\bullet)_3] \cdot 3DMF$ (**1**) and $((CH_3)_2NH_2)_2[Al_4(Cl_2An)_3(Cl_2An^\bullet)_3] \cdot 9DMF$ (**2**), containing ligands in both their dianionic form ($dhbq^{2-}$) as well as in the semiquinonic form ($dhbq^{3-}$). Interestingly, MOFs **1** and **2** were obtained by in situ reduction, using high-throughput methods, which consist of an automated solvothermal equipment with different ligand/Al stoichiometric ratios, in DMF solvent, for optimizing the synthesis conditions. MOFs **1** and **2** show specific surface areas of 1440 and 1430 $m^2g^{-1}$, respectively [65]. A similar MOF was also reported by Harris et al. [62,66], by combining $Fe^{II}$ ions with $H_2Cl_2An$ through a solvothermal reaction in DMF, leading to a novel porous semiquinoid antiferromagnet formulated as $((CH_3)_2NH_2)_2[Fe_2(Cl_2An)_3] \cdot 2H_2O \cdot 6DMF$ (**3**). The chloranilate bridging ligand is simultaneously present in both benzoquinoid and semiquinoid forms, resulting from a spontaneous electron transfer from $Fe^{II}$ to $Cl_2An^{2-}$, giving rise to a mixed-valence layered MOF [62]. The ligand coordinates in its bis-bidentate mode, which generates anionic layers where six metal ions are coordinate by the ligand forming a hexagonal motif, the typical honeycomb packing. The $(CH_3)_2NH_2^+$ cations both balance the charge and orient the anionic layers to an eclipsed structure, forming 1D hexagonal channels, which show a Brunauer–Emmett–Teller (BET) surface area of

1175 m$^2$g$^{-1}$. MOF **3** shows antiferromagnetic interactions with a spontaneous magnetization below 80 K in its solvated form, while the magnetic ordering temperature decreases to 26 K in the desolvated form (**3_desolv**), which shows a BET surface area of 885 m$^2$g$^{-1}$ (Figure 2) and a fully reversible structural contraction consistent with a "breathing" behavior. The high value of magnetic ordering temperature compared to other extended systems containing the same bridging ligand in its dianionic form [45] highlights the ability of semiquinone ligands to form porous magnets with enhanced magnetic coupling between metal ions (*vide supra*) [62]. Moreover, MOFs **3** and **3_desolv** show conductivity values of σ = 1.4(7) × 10$^{-2}$ S/cm (Ea = 0.26(1) eV) and 1.0(3) × 10$^{-3}$ S/cm (Ea = 0.19(1) eV), respectively, proving the ability of benzoquinone derivatives to construct multifunctional MOFs, in which porosity, magnetism, and conductivity coexist [62].
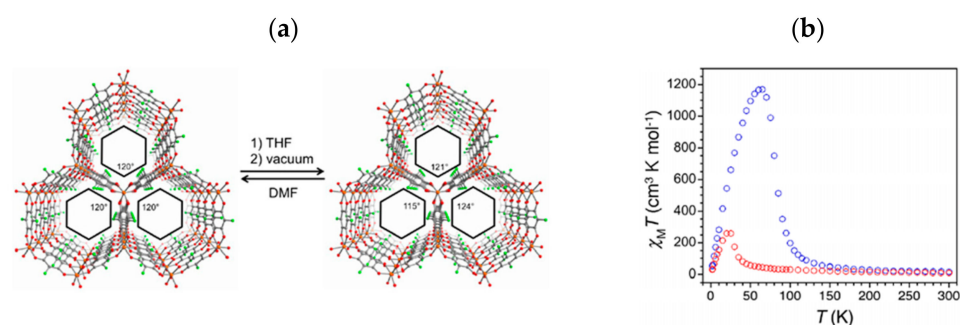


**Figure 2.** (**a**) Perspective view along the *c* axis of crystal structures of MOFs **3** (left) and **3_desolv** (right)—Fe, Cl, O, and C atoms are shown in orange, green, red, and grey, respectively. (**b**) Thermal variation of $\chi_M T$ for MOFs **3** (blue) and **3_desolv** (red) (applied *dc* field of 1000 Oe). Reprinted with permission from Reference [62]. Copyright © 2015, American Chemical Society.

Furthermore, H$_2$Cl$_2$An in MOF **3** could be fully reduced to its semiquinoid form via a post-synthetic approach by using cobaltocene (Cp$_2$Co), which allows a single-crystal-to-single-crystal chemical (one-electron) reduction, due to its porous crystalline structure, affording a 2D MOF, formulated as (Cp$_2$Co)$_{1.43}$((CH$_3$)$_2$NH$_2$)1.57[Fe$_2$ Cl$_2$An $_3$]·4.9DMF (**4**). Remarkably, the Tc can increase up to 105 K, a rare value for MOFs, attributable to the strong magnetic exchange interactions between metal ions mediated by the semiquinone radical form. Variable-field measurements show a magnetic hysteresis up to 100 K, which is consistent with the high Tc value (see Figure 3).
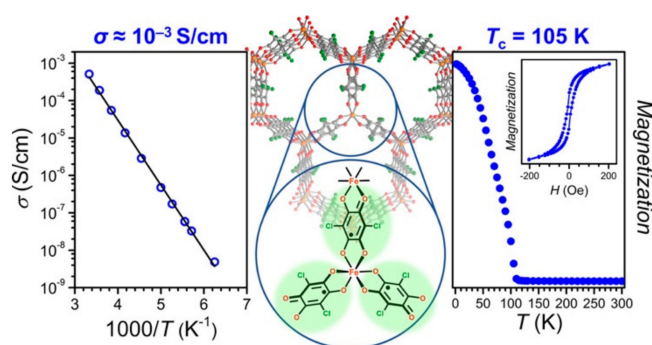


**Figure 3.** Magnetic and transport properties of 2D semiquinoid–based MOF **4**. Reprinted with permission from [66]. Copyright © 2017, American Chemical Society.

The r.t. conductivity of MOF **4**, on a pressed-pellet, has a value of σ = 5.1(3) × 10$^{-4}$ Scm$^{-1}$, probably due to the complete ligand reduction that remove the mixed-valence character of the MOF [66]. Variable-temperature conductivity data in the 300–160 K range fit well the Arrhenius law with E$_a$ = 0.34(1) eV, in agreement with the observed conductivity value of MOF **4** and lower than MOFs **3** and **3_desolv**, supporting the complete chemical reduction.

Noteworthily, the coexistence of high magnetic ordering and electrical conductivity in the same material is rather unusual, as well as the capability of the quinoid MOF to retain its crystalline structure upon post-synthetic chemical reduction, demonstrating the potential of quinoid-based MOFs to provide a new generation of redox-active conducting magnets for future spintronics applications (*vide infra*).

In 2015, Long et al. reported the first example of a 3D dhbq-based MOF, obtained by a solvothermal reaction and formulated as $(NBu_4)_2Fe^{III}_2(dhbq)_3$ (**5**) [67]. This MOF shows a very rare topology for $dhbq^{2-}$-based coordination compounds [68–70] with two interpenetrated (10,3)-*a* networks of opposing chiralities (Figure 4), generating a topology that differs from the classic honeycomb structure frequently observed for anilates [71]. This material behaves as an Arrhenius semiconductor with a very high r.t. conductivity of 0.16(1) S/cm and an Ea of 110 meV. Mössbauer spectroscopy confirms the presence of high-spin $Fe^{III}$ metal ions, and the high conductivity value can be ascribed to the presence of mixed-valency due to $dhbq^{3-}$ radicals, remarkably Class II/III according to Robin-Day, as evidenced by diffuse reflectance measurements in the UV–Vis–NIR range. Noteworthily, MOF **5**, where a $Fe^{II}$-semiquinoid transition occurred, provides a challenging scaffold for constructing tunable long-range electronic communication in MOF [72].
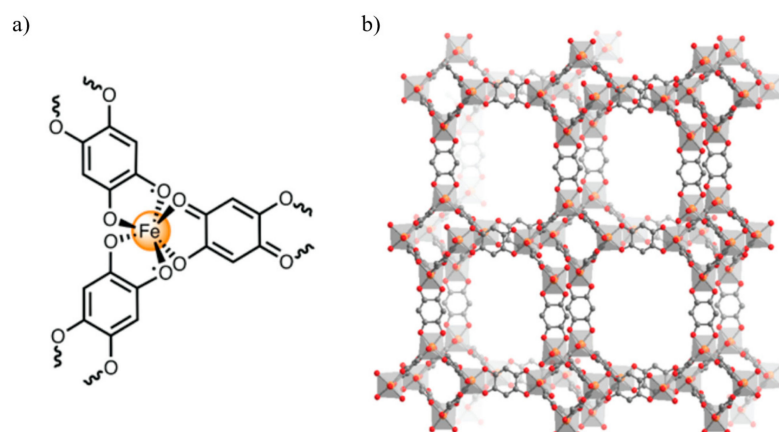


**Figure 4.** (**a**) Molecular structure of a single $Fe^{III}$ center in MOF **5**, showing that two radical ($H_2An^{3-}$) bridging ligands and one diamagnetic ($H_2An^{2-}$) bridging ligand are coordinated to each metal site. (**b**) View of the porous 3D crystal structure formed by $dhbq^{n-}$-bridged $Fe^{III}$ centers, giving the interpenetrated (10,3)-a nets. Reprinted with permission from Reference [67]. Copyright © 2015, American Chemical Society.

Interestingly, it is possible to tune the electrical conductivity by combining dhbq or $H_2Cl_2An$ with transition metal ions having diffuse 3D orbitals. In 2018, Long et al. reported on 2D semiquinoid-bridged frameworks based on titanium, chromium, and vanadium, formulated as $((CH_3)_2NH_2)_2Ti_2(Cl_2An)_3·4.7DMF$ (**6**), $((CH_3)_2NH_2)_{1.5}Cr_2(dhbq)_3·4.4DMF$ (**7**), and $((CH_3)_2NH_2)_2V_2(Cl_2An)_3·6.4DMF$ (**8**), respectively [73]. MOFs **6–8** show a honeycomb-type structure similar to MOFs **1–4**, which were studied electrochemically by using solid-state cyclic voltammetry, which pointed out only ligand-based redox processes for compounds of MOFs **6–7** and a combination of ligand- and metal-based redox activity for MOF **8**. Given their mixed-valence character, they all show electronic conductivity of values $2.7(2) \times 10^{-3}$ S/cm, $1.2(1) \times 10^{-4}$ S/cm, and remarkably 0.45(3) S/cm, respectively, for MOFs **6–8**, following the expected trend based on the correlation with the electronic structure of the frameworks and, in the case of MOF **8**, consistent with the observed metal−ligand covalency [73].

These results show that the incorporation of semiquinoid ligands in an extended scaffold is a valuable strategy for developing multifunctional MOFs with improved electrical conductivity and temperature magnetic ordering, making quinone derivatives excellent candidates for constructing next-generation data processing and storage systems.

## 3. Benzoquinone-Based MOFs

Very recently, Miyasaka et al. reported on post-synthetic generation of radical species via solid-state bulk electrochemistry technique, in a MOF containing diamagnetic benzoquinone derivatives, at the cathode of a lithium-ion battery system (LIB), producing a radical spin in the benzoquinone moiety and $Li^+$ insertion for preserving neutrality [74]. In this case, porosity is a fundamental requirement for host $Li^+$ ions. The precursor, formulated as $(H_3O)_2(phz)_3[Fe_2(Cl_2An)_3]$ (**9**), was obtained by the desolvatation of $(H_3O)_2(phz)_3[Fe_2(Cl_2An)_3]\cdot(CH_3COCH_3)_n\cdot(H_2O)_n$ (9_solv). MOF **9** shows the typical honeycomb packing shown by anilates, with alternating anionic/cationic layers, where the counter cations $[(H_3O)_2(phz)_3]^{2+}$ are placed between the layers, acting as a templating agent that leads to 1D hexagonal channels along the *c* axis, conferring porosity to the network. MOF **9** shows paramagnetic behavior and short-range ferromagnetic correlations among $Fe^{II}$ ions, through a chloranilate linker, in the layered framework, as can be seen by lack of hysteresis in the magnetization vs. field (M-H) measurements, even at 5 K. With the ligand reduction due to the insertion of $Li^+$ ions, antiferromagnetic superexchange interactions between the radical anion $Cl_2An\bullet^{3-}$ and $Fe^{II}$ ions took place, and the reduced MOF, formulated as $(Li)_3(H_3O)_2(phz)_3[(Fe)_2(Cl_2An)_3]$ (**9_red**), shows one of the higher $T_c$ values reported so far, Tc = 128 K [74] (Figure 5). The formation of the radical ligand $Cl_2An\bullet^{3-}$, starting from $Cl_2An^{2-}$, leads to a long-range magnetic ordering in the MOF, making this MOF a potential cathode material of a LIB.
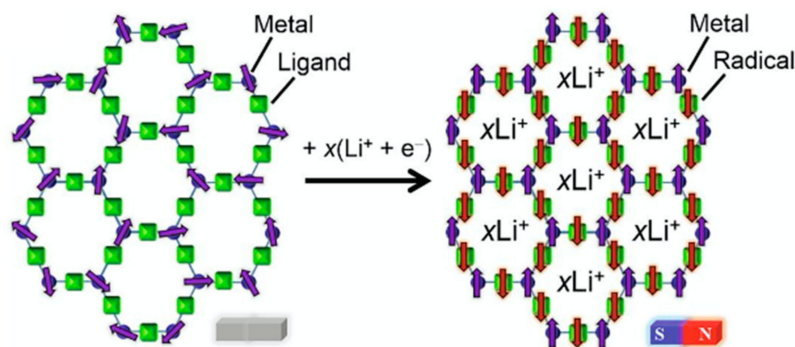


**Figure 5.** Schematic view of spin variation during the discharge process MOF → electron-reduced MOF, $(Li^+)_x[MOF]^{x-}$. Reprinted with permission from Reference [74].

Remarkably, Harris et al. [75] reported on the simultaneous switching of magnetic and conducting properties induced by post-synthetic chemical reduction in a MOF of formula $(Me_4N)_2[Mn_2(Cl_2An)_3]x.DMF$, containing the diamagnetic chloranilate linker (**10**). When MOF **10** is soaked in a THF equimolar reducing solution of sodium naphthalenide and 1,2-dihydroacenaphthylene for several days, a semiquinoid-based MOF, of formula $Na_3(Me_4N)_2[Mn_2(Cl_2An)_3]3.9THF$ (**11**), is obtained. The reduction mechanism occurs via single-crystal-to-single-crystal process (*vide infra*), provoking the formation of $Cl_2An\bullet^{3-}$ semiquinone radical form starting from diamagnetic $Cl_2An^{2-}$, while the oxidation state of $Mn^{II}$ remains unchanged. Upon the conversion in the radical form of $Cl_2An^{2-}$, a simultaneous change in both conductivity and magnetic properties is observed. Indeed MOF **10** shows a paramagnetic behavior above 1.8 K and a r.t. conductivity value of $\sigma = 1.14(3) \times 10^{-13}$ Scm$^{-1}$ ($E_a = 0.74(3)$ eV), whereas MOF **11** shows antiferromagnetic interactions between $Mn^{II}$ ions below 41 K, mediated by the semiquinone, and a r.t. conductivity value of $\sigma = 2.27(1) \times 10^{-8}$ Scm$^{-1}$ ($E_a = 0.489(8)$ eV), a value 200,000 times higher than the respective benzoquinoid framework. Furthermore, by soaking MOF **11** in ferrocene ($Cp_2Fe^+$) solution, a compound, formulated as $Na((CH_3)_4N)[Mn_2(Cl_2An)_3]$ 5.5THF 0.8CH$_3$CN (**12**), is afforded, showing similar values of $T_c$ and $\sigma$ as MOF **10** (oxidized compound), highlighting the reversibility of the redox process [75], as reported in Figure 6.
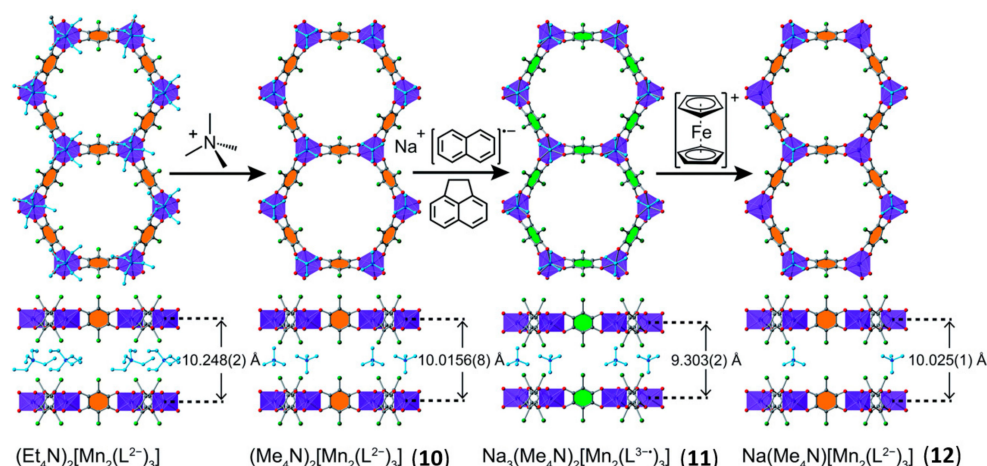
**Figure 6.** Schematic representation of reversible redox mechanism via single-crystal-to-single-crystal (SC-SC) process in MOFs **10–12**. Reproduced from Reference [75] with permission from the Royal Society of Chemistry.

The capability of benzoquinone-based MOFs to undergo reversible redox processes, which provoke a simultaneous switching of magnetic and transport properties, are worth being highlighted, as they may be considered suitable materials for future spintronic technologies.

## 4. Conclusions and Perspectives

The recent developments on redox-active benzoquinone-based MOFs, herein discussed, contribute to the ongoing research on the use of these materials for technologically relevant applications. It turns out that benzoquinoid/semiquinoid redox activity is a powerful strategy to tune their physical properties, in particular magnetism and/or conductivity. Porosity is a remarkable additional property and porous channels in benzoquinoid MOFs, allowing for the facile insertion/extraction of the electrolytes, which makes them promising materials for electrodes and rechargeable energy storage systems [76,77]. Furthermore, it has been highlighted that post-synthetic chemical redox reactions are a promising strategy to control ligand redox states in the MOF and the related changes of its conducting and magnetic properties, while the scaffold with metal–semiquinoid transitions provides tunable and delocalized electronic structures. Therefore, the whole redox control over MOFs is a very challenging task, specifically for their applications in the electronic devices realm. In more detail, redox control requires open-shell ligands and metals, frontier orbitals with similar energies, and maximal overlap to favor charge delocalization, and benzoquinones successfully match these requirements. Finally, the fabrication of semiquinoid MOFs, showing coexistence of simultaneously switchable conducting and magnetic properties, represents a forefront challenge for their potential applications in next-generation spintronic technologies, as magnetic transistors, terahertz information, and multifunctional chips, where data storage and information processing can occur at the same location.

**Author Contributions:** N.M., M.O. and S.A.S. contributed equally in terms of accurate literature searching and paper writing; M.L.M. supervised and wrote the paper with the help of N.M. All authors have read and agreed to the published version of the manuscript.

**Conflicts of Interest:** The authors declare no conflict of interest.

# References

1. Tran, M.; Kline, K.; Qin, Y.; Shen, Y.; Green, M.D.; Tongay, S. 2D coordination polymers: Design guidelines and materials perspective. *Appl. Phys. Rev.* **2019**, *6*, 041311. [CrossRef]
2. Mercuri, M.L.; Congiu, F.; Concas, G.; Ashoka Sahadevan, S. Recent Advances on Anilato-Based Molecular Materials with Magnetic and/or Conducting Properties. *Magnetochemistry* **2017**, *3*, 17. [CrossRef]
3. Coronado, E.; Galán-Mascarós, J.R.; Gómez-García, C.J.; Laukhin, V. Coexistence of ferromagnetism and metallic conductivity in a molecule-based layered compound. *Nature* **2000**, *408*, 447–449. [CrossRef]
4. Haldar, R.; Heinke, L.; Wöll, C. Advanced Photoresponsive Materials Using the Metal–Organic Framework Approach. *Adv. Mater.* **2019**, *1905227*, 1905227. [CrossRef]
5. Bénard, S.; Yu, P.; Audière, J.P.; Rivière, E.; Clément, R.; Guilhem, J.; Tchertanov, L.; Nakatani, K. Structure and NLO properties of layered bimetallic oxalato-bridged ferromagnetic networks containing stilbazolium-shaped chromophores. *J. Am. Chem. Soc.* **2000**, *122*, 9444–9454. [CrossRef]
6. Han, C.; Li, H.; Shi, R.; Zhang, T.; Tong, J.; Li, J.; Li, B. Organic quinones towards advanced electrochemical energy storage: Recent advances and challenges. *J. Mater. Chem. A* **2019**, *7*, 23378–23415. [CrossRef]
7. Pamei, M.; Puzari, A. Luminescent transition metal–organic frameworks: An emerging sensor for detecting biologically essential metal ions. *Nano-Struct. Nano-Objects* **2019**, *19*, 100364–100386. [CrossRef]
8. Ashoka Sahadevan, S.; Monni, N.; Abhervé, A.; Marongiu, D.; Sarritzu, V.; Sestu, N.; Saba, M.; Mura, A.; Bongiovanni, G.; Cannas, C.; et al. Nanosheets of Two-Dimensional Neutral Coordination Polymers Based on Near-Infrared-Emitting Lanthanides and a Chlorocyananilate Ligand. *Chem. Mater.* **2018**, *30*, 6575–6586. [CrossRef]
9. Kuznetsova, A.; Matveevskaya, V.; Pavlov, D.; Yakunenkov, A.; Potapov, A. Coordination polymers based on highly emissive ligands: Synthesis and functional properties. *Materials* **2020**, *13*, 2699. [CrossRef]
10. He, Y.; Chen, F.; Li, B.; Qian, G.; Zhou, W.; Chen, B. Porous metal–organic frameworks for fuel storage. *Coord. Chem. Rev.* **2018**, *373*, 167–198. [CrossRef]
11. Zhang, X.; Chen, A.; Zhong, M.; Zhang, Z.; Zhang, X.; Zhou, Z.; Bu, X.-H. *Metal–Organic Frameworks (MOFs) and MOF-Derived Materials for Energy Storage and Conversion*; Springer: Singapore, 2019; Volume 2, ISBN 0123456789.
12. Koo, W.-T.; Jang, J.-S.; Kim, I.-D. Metal-Organic Frameworks for Chemiresistive Sensors. *Chem* **2019**, *5*, 1938–1963. [CrossRef]
13. Baumann, A.E.; Burns, D.A.; Liu, B.; Thoi, V.S. Metal-organic framework functionalization and design strategies for advanced electrochemical energy storage devices. *Commun. Chem.* **2019**, *2*, 1–14. [CrossRef]
14. Oggianu, M.; Monni, N.; Mameli, V.; Cannas, C.; Sahadevan, S.A.; Mercuri, M.L. Designing Magnetic NanoMOFs for Biomedicine: Current Trends and Applications. *Magnetochemistry* **2020**, *6*, 39. [CrossRef]
15. Mínguez Espallargas, G.; Coronado, E. Magnetic functionalities in MOFs: From the framework to the pore. *Chem. Soc. Rev.* **2018**, *47*, 533–557. [CrossRef]
16. Wang, H.; Cui, L.; Xie, J.; Leong, C.F.; Alessandro, D.M.D.; Zuo, J. Functional coordination polymers based on redox-active tetrathiafulvalene and its derivatives. *Coord. Chem. Rev.* **2017**, *345*, 342–361. [CrossRef]
17. Degayner, J.A.; Wang, K.; Harris, T.D. A Ferric Semiquinoid Single-Chain Magnet via Thermally-Switchable Metal-Ligand Electron Transfer. *J. Am. Chem. Soc.* **2018**, *140*, 6550–6553. [CrossRef]
18. Sun, L.; Hendon, C.H.; Park, S.S.; Tulchinsky, Y.; Wan, R.; Wang, F.; Walsh, A.; Dinca, M. Is iron unique in promoting electrical conductivity in MOFs? *Chem. Sci.* **2017**, *8*, 4450–4457. [CrossRef] [PubMed]
19. Halls, J.E.; Jiang, D.; Burrows, A.D.; Kulandainathan, M.A.; Marken, F. Electrochemistry within metal-organic frameworks. *Electrochemistry* **2013**, *12*, 187–210. [CrossRef]
20. Calbo, J.; Golomb, M.J.; Walsh, A. Redox-active metal-organic frameworks for energy conversion and storage. *J. Mater. Chem. A* **2019**, *7*, 16571–16597. [CrossRef]
21. D'Alessandro, D.M. Exploiting redox activity in metal-organic frameworks: Concepts, trends and perspectives. *Chem. Commun.* **2016**, *52*, 8957–8971. [CrossRef] [PubMed]
22. Pedersen, K.S.; Perlepe, P.; Aubrey, M.L.; Woodruff, D.N.; Reyes-Lillo, S.E.; Reinholdt, A.; Voigt, L.; Li, Z.; Borup, K.; Rouzieres, M.; et al. Formation of the layered conductive magnet $CrCl_2$(pyrazine)$_2$ through redox-active coordination chemistry. *Nat. Chem.* **2018**, *10*, 1056–1061. [CrossRef] [PubMed]
23. Yan, Y.; Keating, C.; Chandrasekaran, P.; Jayarathne, U.; Mague, J.T.; Debeer, S.; Lancaster, K.M.; Sproules, S.; Rubtsov, I.V.; Donahue, J.P. Ancillary ligand effects upon dithiolene redox noninnocence in tungsten Bis(dithiolene) complexes. *Inorg. Chem.* **2013**, *52*, 6743–6751. [CrossRef]
24. Ellis, H.; Eriksson, S.K.; Feldt, S.M.; Gabrielsson, E.; Lohse, P.W.; Lindblad, R.; Sun, L.; Rensmo, H.; Boschloo, G.; Hagfeldt, A. Linker unit modification of triphenylamine-based organic dyes for efficient cobalt mediated dye-sensitized solar cells. *J. Phys. Chem. C* **2013**, *117*, 21029–21036. [CrossRef]
25. Li, C.; Shi, L.; Zhang, L.; Chen, P.; Zhu, J.; Wang, X.; Fu, Y. Ultrathin two-dimensional $\pi$–d conjugated coordination polymer Co3(hexaaminobenzene)2 nanosheets for highly efficient oxygen evolution. *J. Mater. Chem.* **2020**, *8*, 369–379. [CrossRef]
26. Campbell, W.M.; Jolley, K.W.; Wagner, P.; Wagner, K.; Walsh, P.J.; Gordon, K.C.; Schmidt-Mende, L.; Nazeeruddin, M.K.; Wang, Q.; Grätzel, M.; et al. Highly efficient porphyrin sensitizers for dye-sensitized solar cells. *J. Phys. Chem. C* **2007**, *111*, 11760–11762. [CrossRef]

27. Xiang, W.; Huang, F.; Cheng, Y.B.; Bach, U.; Spiccia, L. Aqueous dye-sensitized solar cell electrolytes based on the cobalt(ii)/(iii) tris(bipyridine) redox couple. *Energy Environ. Sci.* **2013**, *6*, 121–127. [CrossRef]

28. Su, J.; Hu, T.H.; Murase, R.; Wang, H.Y.; D'Alessandro, D.M.; Kurmoo, M.; Zuo, J.L. Redox Activities of Metal-Organic Frameworks Incorporating Rare-Earth Metal Chains and Tetrathiafulvalene Linkers. *Inorg. Chem.* **2019**, *58*, 3698–3706. [CrossRef]

29. Wu, Y.; Zeng, R.; Nan, J.; Shu, D.; Qiu, Y.; Chou, S.L. Quinone Electrode Materials for Rechargeable Lithium/Sodium Ion Batteries. *Adv. Energy Mater.* **2017**, *7*, 1700278–1700304. [CrossRef]

30. Tabor, D.P.; Gómez-Bombarelli, R.; Tong, L.; Gordon, R.G.; Aziz, M.J.; Aspuru-Guzik, A. Mapping the frontiers of quinone stability in aqueous media: Implications for organic aqueous redox flow batteries. *J. Mater. Chem. A* **2019**, *7*, 12833–12841. [CrossRef]

31. Boota, M.; Chen, C.; Be, M.; Miao, L.; Gogotsi, Y. Pseudocapacitance and excellent cyclability of 2,5-dimethoxy-1,4-benzoquinone on graphene. *Energy Environ. Sci.* **2016**, *9*, 2586–2594. [CrossRef]

32. Schon, T.B.; Mcallister, B.T.; Li, P.; Seferos, D.S. The rise of organic electrode materials for energy storage. *Chem. Soc. Rev.* **2016**, *45*, 6345–6404. [CrossRef]

33. Patai, S.; Rappoport, Z. *The Chemistry of the Quinonoid Compounds*; Bath, John Wiles & Sons Ltd.: Hoboken, NJ, USA, 1988; Volume 2.

34. Guin, P.S.; Das, S.; Mandal, P.C. Electrochemical Reduction of Quinones in Different Media: A Review. *Int. J. Electrochem.* **2011**, *2011*, 1–22. [CrossRef]

35. Lehmann, M.W.; Evans, D.H. Mechanism of the electrochemical reduction of 3,5-di-tert-butyl-1,2-benzoquinone. Evidence for a concerted electron and proton transfer reaction involving a hydrogen-bonded complex as reactant. *J. Phys. Chem. B* **2001**, *105*, 8877–8884. [CrossRef]

36. Gupta, N.; Linschitz, H. Hydrogen-bonding and protonation effects in electrochemistry of quinones in aprotic solvents. *J. Am. Chem. Soc.* **1997**, *119*, 6384–6391. [CrossRef]

37. Given, P.H.; Peover, M.E. Polarographic Reduction of Aromatic Hydrocarbons and Carbonyl Compounds in Dimethylformamide in the Presence of Proton-donors. *J. Chem. Soc.* **1960**, 385–393. [CrossRef]

38. Wightman, R.M.; Cockrell, J.R.; Murray, R.W.; Burnett, J.N.; Jones, S.B. Protonation Kinetics and Mechanism for 1,8-Dihydroxyanthraquinone and Anthraquinone Anion Radicals in Dimethylformamide Solvent. *J. Am. Chem. Soc.* **1976**, *98*, 2562–2570. [CrossRef]

39. Garza, J.; Vargas, R.; Gómez, M.; González, I.; González, F.J. Theoretical and Electrochemical Study of the Quinone-Benzoic Acid Adduct Linked by Hydrogen Bonds. *J. Phys. Chem. A* **2003**, *107*, 11161–11168. [CrossRef]

40. Yao, M.; Senoh, H.; Yamazaki, S.I.; Siroma, Z.; Sakai, T.; Yasuda, K. High-capacity organic positive-electrode material based on a benzoquinone derivative for use in rechargeable lithium batteries. *J. Power Sources* **2010**, *195*, 8336–8340. [CrossRef]

41. Khattak, A.M.; Ghazi, Z.A.; Liang, B.; Khan, N.A.; Iqbal, A.; Li, L.; Tang, Z. A redox-active 2D covalent organic framework with pyridine moieties capable of faradaic energy storage. *J. Mater. Chem. A* **2016**, *4*, 16312–16317. [CrossRef]

42. Atzori, M.; Pop, F.; Cauchy, T.; Mercuri, M.L.; Avarvari, N. Thiophene-benzoquinones: Synthesis, crystal structures and preliminary coordination chemistry of derived anilate ligands. *Org. Biomol. Chem.* **2014**, *12*, 8752–8763. [CrossRef]

43. Atzori, M.; Artizzu, F.; Sessini, E.; Marchiò, L.; Loche, D.; Serpe, A.; Deplano, P.; Concas, G.; Pop, F.; Avarvari, N.; et al. Halogen-bonding in a new family of tris(haloanilato)metallate(III) magnetic molecular building blocks. *Dalton Trans.* **2014**, *43*, 7006–7019. [CrossRef]

44. Abhervé, A.; Mañas-Valero, S.; Clemente-León, M.; Coronado, E. Graphene related magnetic materials: Micromechanical exfoliation of 2D layered magnets based on bimetallic anilate complexes with inserted [Fe$^{III}$ (acac 2 -trien)] + and [Fe$^{III}$ (sal 2 -trien)] + molecules. *Chem. Sci.* **2015**, *6*, 4665–4673. [CrossRef]

45. Atzori, M.; Benmansour, S.; Mínguez Espallargas, G.; Clemente-León, M.; Abhervé, A.; Gómez-Claramunt, P.; Coronado, E.; Artizzu, F.; Sessini, E.; Deplano, P.; et al. A family of layered chiral porous magnets exhibiting tunable ordering temperatures. *Inorg. Chem.* **2013**, *52*, 10031–10040. [CrossRef]

46. Benmansour, S.; Abhervé, A.; Gómez-Claramunt, P.; Vallés-García, C.; Gómez-García, C.J. Nanosheets of Two-Dimensional Magnetic and Conducting Fe(II)/Fe(III) Mixed-Valence Metal-Organic Frameworks. *ACS Appl. Mater. Interfaces* **2017**, *9*, 26210–26218. [CrossRef]

47. Sahadevan, S.A.; Abhervé, A.; Monni, N.; Sáenz De Pipaón, C.; Galán-Mascarós, J.R.; Waerenborgh, J.C.; Vieira, B.J.C.; Auban-Senzier, P.; Pillet, S.; Bendeif, E.-E.; et al. Conducting Anilate-Based Mixed-Valence Fe(II)Fe(III) Coordination Polymer: Small-Polaron Hopping Model for Oxalate-Type Fe(II)Fe(III) 2D Networks. *J. Am. Chem. Soc.* **2018**, *140*, 12611–12621. [CrossRef] [PubMed]

48. Atzori, M.; Pop, F.; Auban-Senzier, P.; Gómez-García, C.J.; Canadell, E.; Artizzu, F.; Serpe, A.; Deplano, P.; Avarvari, N.; Mercuri, M.L. Structural diversity and physical properties of paramagnetic molecular conductors based on bis(ethylenedithio) tetrathiafulvalene (BEDT-TTF) and the tris(chloranilato)ferrate(III) complex. *Inorg. Chem.* **2014**, *53*, 7028–7039. [CrossRef]

49. Kitagawa, S.; Kawata, S. Coordination compounds of 1,4-dihydroxybenzoquinone and its homologues. Structures and properties. *Coord. Chem. Rev.* **2002**, *224*, 11–34. [CrossRef]

50. Nielson, K.V.; Zhang, L.; Zhang, Q.; Liu, T.L. A strategic high yield synthesis of 2,5-dihydroxy-1,4-benzoquinone Based MOFs. *Inorg. Chem.* **2019**, *58*, 10756–10760. [CrossRef] [PubMed]

51. Poschmann, M.P.M.; Reinsch, H.; Stock, N. [$M_2$(μ-OH)$_2$(DHBQ)$_3$] (M = Zr, Hf)—Two New Isostructural Coordination Polymers based on the Unique $M_2O_{14}$ Inorganic Building Unit and 2,5-Dioxido-p-benzoquinone as Linker Molecule. *Z. Anorg. Und Allg. Chem.* **2021**, *647*, 436–441. [CrossRef]

52. Benmansour, S.; Hernández-Paredes, A.; Gómez-García, C.J. Effect of the lanthanoid-size on the structure of a series of lanthanoid-anilato 2-D lattices. *J. Coord. Chem.* **2018**, *71*, 845–863. [CrossRef]

53. Gómez-Claramunt, P.; Benmansour, S.; Hernández-Paredes, A.; Cerezo-Navarrete, C.; Rodríguez-Fernández, C.; Canet-Ferrer, J.; Cantarero, A.; Gómez-García, C.J. Tuning the Structure and Properties of Lanthanoid Coordination Polymers with an Asymmetric Anilato Ligand. *Magnetochemistry* **2018**, *4*, 6. [CrossRef]

54. Benmansour, S.; Pérez-Herráez, I.; López-Martínez, G.; Gómez García, C.J. Solvent-modulated structures in anilato-based 2D coordination polymers. *Polyhedron* **2017**, *135*, 17–25. [CrossRef]

55. Kingsbury, C.J.; Abrahams, B.F.; Auckett, J.E.; Chevreau, H.; Dharma, A.D.; Duyker, S.; He, Q.; Hua, C.; Hudson, T.A.; Murray, K.S.; et al. Square Grid Metal—Chloranilate Networks as Robust Host Systems for Guest Sorption. *Chem. Eur. J.* **2019**, *25*, 5222–5234. [CrossRef]

56. Sahadevan, S.A.; Monni, N.; Abhervé, A.; Cosquer, G.; Oggianu, M.; Ennas, G.; Yamashita, M.; Avarvari, N.; Mercuri, M.L. Dysprosium Chlorocyanoanilate-Based 2D-Layered Coordination Polymers. *Inorg. Chem.* **2019**, *58*, 13988–13998. [CrossRef]

57. Benmansour, S.; Gómez-García, C.J. Lanthanoid-anilato complexes and lattices. *Magnetochemistry* **2020**, *6*, 71. [CrossRef]

58. Benmansour, S.; Hernández-Paredes, A.; Bayona-Andrés, M.; Gómez-García, C.J. Slow Relaxation of the Magnetization in Anilato-Based Dy(III) 2D Lattices. *Molecules* **2021**, *26*, 1190. [CrossRef] [PubMed]

59. Kawata, S.; Kitagawa, S.; Kumagai, H.; Kudo, C.; Kamesaki, H.; Ishiyama, T.; Suzuki, R.; Kondo, M.; Katada, M. Rational Design of a Novel Intercalation System. Layer-Gap Control of Crystalline Coordination Polymers, {[Cu(CA)(H2O)m](G)}n (m = 2,5 = 2,5-Dimethylpyrazine and Phenazine; m = 1, G = 1,2,3,4,6,7,8,9-Octahydrophenazine). *Inorg. Chem.* **1996**, *35*, 4449–4461. [CrossRef] [PubMed]

60. Maka, V.K.; Mukhopadhyay, A.; Jindal, S.; Moorthy, J.N. Redox-Reversible 2D Metal–Organic Framework Nanosheets (MONs) Based on the Hydroquinone/Quinone Couple. *Chem. A Eur. J.* **2019**, *25*, 3835–3842. [CrossRef]

61. Zhu, X.Q.; Wang, C.H. Accurate estimation of the one-electron reduction potentials of various substituted quinones in DMSO and CH3CN. *J. Org. Chem.* **2010**, *75*, 5037–5047. [CrossRef] [PubMed]

62. Jeon, I.R.; Negru, B.; Van Duyne, R.P.; Harris, T.D. A 2D Semiquinone Radical-Containing Microporous Magnet with Solvent-Induced Switching from Tc = 26 to 80 K. *J. Am. Chem. Soc.* **2015**, *137*, 15699–15702. [CrossRef]

63. Abrahams, B.F.; Bond, A.M.; Le, T.H.; McCormick, L.J.; Nafady, A.; Robson, R.; Vo, N. Voltammetric reduction and re-oxidation of solid coordination polymers of dihydroxybenzoquinone. *Chem. Commun.* **2012**, *48*, 11422–11424. [CrossRef]

64. Kharitonov, A.D.; Trofimova, O.Y.; Meshcheryakova, I.N.; Fukin, G.K.; Khrizanforov, M.N.; Budnikova, Y.H.; Bogomyakov, A.S.; Aysin, R.R.; Kovalenko, K.A.; Piskunov, A.V. 2D-metal-organic coordination polymers of lanthanides (La(III), Pr(III) and Nd(III)) with redox-active dioxolene bridging ligands. *CrystEngComm* **2020**, *22*, 4675–4679. [CrossRef]

65. Halis, S.; Inge, A.K.; Dehning, N.; Weyrich, T.; Reinsch, H.; Stock, N. Dihydroxybenzoquinone as Linker for the Synthesis of Permanently Porous Aluminum Metal-Organic Frameworks. *Inorg. Chem.* **2016**, *55*, 7425–7431. [CrossRef]

66. DeGayner, J.A.; Jeon, I.R.; Sun, L.; Dincă, M.; Harris, T.D. 2D Conductive Iron-Quinoid Magnets Ordering up to Tc = 105 K via Heterogenous Redox Chemistry. *J. Am. Chem. Soc.* **2017**, *139*, 4175–4184. [CrossRef]

67. Darago, L.E.; Aubrey, M.L.; Yu, C.J.; Gonzalez, M.I.; Long, J.R. Electronic Conductivity, Ferrimagnetic Ordering, and Reductive Insertion Mediated by Organic Mixed-Valence in a Ferric Semiquinoid Metal-Organic Framework. *J. Am. Chem. Soc.* **2015**, *137*, 15703–15711. [CrossRef]

68. Benmansour, S.; Vallés-García, C.; Gómez-Claramunt, P.; Mínguez Espallargas, G.; Gómez-García, C.J. 2D and 3D Anilato-Based Heterometallic M(I)M(III) Lattices: The Missing Link. *Inorg. Chem.* **2015**, *54*, 5410–5418. [CrossRef]

69. Barltrop, J.A.; Burstall, M.L. The synthesis of Tetracyclines. Part I. Some Model Diene Reactions. *J. Chem. Soc.* **1959**, 2183–2186. [CrossRef]

70. Abrahams, B.F.; Hudson, T.A.; McCormick, L.J.; Robson, R. Coordination polymers of 2,5-dihydroxybenzoquinone and chloranilic acid with the (10,3)- A topology. *Cryst. Growth Des.* **2011**, *11*, 2717–2720. [CrossRef]

71. Luo, T.-T.; Liu, Y.-H.; Tsai, H.-L.; Su, C.-C.; Ueng, C.-H.; Lu, K.-L. A Novel Hybrid Supramolecular Network Assembled from Perfect p-p Stacking of an Anionic Inorganic Layer and a Cationic Hydronium-Ion-Mediated Organic Layer. *Eur. J. Inorg. Chem.* **2004**, *2004*, 4253–4258. [CrossRef]

72. Miller, J.S. Magnetically ordered molecule-based materials. *Chem. Soc. Rev.* **2011**, *40*, 3266–3296. [CrossRef]

73. Ziebel, M.E.; Darago, L.E.; Long, J.R. Control of Electronic Structure and Conductivity in Two-Dimensional Metal-Semiquinoid Frameworks of Titanium, Vanadium, and Chromium. *J. Am. Chem. Soc.* **2018**, *140*, 3040–3051. [CrossRef] [PubMed]

74. Chen, J.; Taniguchi, K.; Sekine, Y.; Miyasaka, H. Electrochemical development of magnetic long-range correlations with Tc = 128 K in a tetraoxolene-bridged Fe-based framework. *J. Magn. Magn. Mater.* **2020**, *494*, 165818. [CrossRef]

75. Liu, L.; Degayner, J.A.; Sun, L.; Zee, D.Z.; Harris, T.D. Reversible redox switching of magnetic order and electrical conductivity in a 2D manganese benzoquinoid framework. *Chem. Sci.* **2019**, *10*, 4652–4661. [CrossRef] [PubMed]

76.  Taniguchi, K.; Chen, J.; Sekine, Y.; Miyasaka, H. Magnetic Phase Switching in a Tetraoxolene-Bridged Honeycomb Ferrimagnet Using a Lithium Ion Battery System. *Chem. Mater.* **2017**, *29*, 10053–10059. [CrossRef]
77.  Jiang, Q.; Xiong, P.; Liu, J.; Xie, Z.; Wang, Q.; Yang, X.Q.; Hu, E.; Cao, Y.; Sun, J.; Xu, Y.; et al. A Redox-Active 2D Metal–Organic Framework for Efficient Lithium Storage with Extraordinary High Capacity. *Angew. Chem. Int. Ed.* **2020**, *59*, 5273–5277. [CrossRef]